Available online at www.sciencedirect.com
ScienceDirect
Applied Geochemistry 22 (2007) 90–108
Applied Geochemistry
www.elsevier.com/locate/apgeochem

Using dissolved gas analysis to investigate the performance of an organic carbon permeable reactive barrier for the treatment of mine drainage

R.L. Williams [a,1], K.U. Mayer [a,*], R.T. Amos [a], D.W. Blowes [b], C.J. Ptacek [b,c], J.G. Bain [b]

[a] Department of Earth and Ocean Sciences, University of British Columbia, 6339 Stores Road, Vancouver, BC, Canada V6T 1Z4
[b] Department of Earth Sciences, University of Waterloo, Waterloo, ON, Canada N2L 3G1
[c] Environment Canada, Burlington, ON, Canada L7R 4A6

Received 7 September 2005; accepted 14 September 2006
Editorial handling by R. Fuge
Available online 21 November 2006

Abstract

The strongly reducing nature of permeable reactive barrier (PRB) treatment materials can lead to gas production, potentially resulting in the formation of gas bubbles and ebullition. Degassing in organic C based PRB systems due to the production of gases (primarily CO_2 and CH_4) is investigated using the depletion of naturally occurring non-reactive gases Ar and N_2, to identify, confirm, and quantify chemical and physical processes. Sampling and analysis of dissolved gases were performed at the Nickel Rim Mine Organic Carbon PRB, which was designed for the treatment of groundwater contaminated by low quality mine drainage characterized by slightly acidic pH, and elevated Fe(II) and SO_4 concentrations. A simple 4-gas degassing model was used to analyze the dissolved gas data, and the results indicate that SO_4 reduction is by far the dominant process of organic C consumption within the barrier. The data provided additional information to delineate rates of microbially mediated SO_4 reduction and confirm the presence of slow and fast flow zones within the barrier. Degassing was incorporated into multicomponent reactive transport simulations for the barrier and the simulations were successful in reproducing observed dissolved gas trends.

1. Introduction

Permeable reactive barriers (PRBs) offer a passive approach for the remediation of contaminated groundwater. These remediation systems are often composed of treatment mixtures containing zero-valent Fe (Fe^0) or organic C-based materials, with the objective of inducing reducing conditions which are suitable for the treatment of a variety of contaminants (Blowes et al., 1997, 2000; Benner et al., 1999; Schipper and Vojvodić-Vuković, 2001). The strongly reducing nature of treatment materials may lead to gas production in permeable reactive barriers (PRB's), potentially resulting in the formation of gas bubbles and ebullition.

* Corresponding author. Tel.: +1 604 822 1539; fax: +1 604 822 6088.
E-mail address: umayer@eos.ubc.ca (K.U. Mayer).
[1] Present address: BGC Engineering Inc., 500-1045 Howe Street, Vancouver, BC, Canada V6Z 2A9.

0883-2927/$ - see front matter © 2006 Elsevier Ltd. All rights reserved.
doi:10.1016/j.apgeochem.2006.09.007

The formation of gas bubbles has been observed previously in laboratory columns containing organic materials (Soares et al., 1988, 1991) and Fe^0 (Kamolpornwijit et al., 2003). Mackenzie et al. (1999) demonstrated that H_2 gas production and entrapment could occur within Fe media. Long-term column studies conducted by Vikesland et al. (2003) showed that precipitate formation and gas pocket accumulation could alter transport properties of a column filled with granular Fe media. The vertical transport conditions of most column experiments; however, do not correspond to field conditions, and gas bubble formation, entrapment, exsolution, and ebullition are expected to be different in field situations (Vikesland et al., 2003).

Although gas production may have negative effects on barrier permeability (Mackenzie et al., 1999; Fryar and Schwartz, 1998; Kamolpornwijit et al., 2003) and contaminant treatment (Vikesland et al., 2003; Morrison, 2003), the formation of gas bubbles will also affect the gas composition in the pore water, and therefore may be a useful indicator in helping to delineate physical transport and biogeochemical reaction processes occurring within and down-gradient of PRB systems. Precipitation water is typically in equilibrium with atmospheric gases prior to infiltration into the subsurface. Subsequently, microbially mediated processes may either consume gases (O_2 by aerobic respiration, H_2 coupled with the reduction of various electron acceptors) or produce gases (e.g.: N_2 by denitrification, H_2S and CO_2 by SO_4 reduction, volatile organic S compounds (VOSCs) by anaerobic methylation of sulfide (Finster et al., 1990), CH_4 and CO_2 by methanogenesis, H_2 by organic matter fermentation, and NH_3 by NO_3 reduction). Some of these gases (VOSCs, H_2) are reaction intermediates and are not expected to accumulate in significant concentrations in organic C based PRBs, while the generation of other gases such as CH_4, CO_2, and H_2S may significantly alter the dissolved gas composition. Inorganic reactions, such as carbonate mineral dissolution–precipitation may also affect the ratio of gases dissolved in groundwater.

Blicher-Mathiesen et al. (1998) demonstrated that naturally occurring non-reactive dissolved gases (i.e., Ar) could be used to estimate the degree of denitrification and degassing taking place within a Danish riparian wetland. Amos et al. (2005) used non-reactive dissolved gases at a petroleum hydrocarbon contaminated site as reaction and transport tracers. These authors also demonstrated that when denitrification is negligible, Ar and N_2 could be used effectively to better understand and quantify physical and chemical processes related to methanogenic activity. Specifically, Amos et al. (2005) showed that the production of CH_4 can induce degassing, thus causing depletion of dissolved Ar and N_2. The degree of Ar and N_2 depletion could be used to infer historical CH_4 production in the contaminated zone, while the correlation between decreasing CH_4 concentrations and the recovery of Ar and N_2 to background concentrations suggested that attenuation of CH_4 in the down gradient aquifer is at least in part controlled by physical processes. Fortuin and Willemsen (2005) used the hydrogeochemical transport model PHREEQC to simulate organic C decomposition, CH_4 formation and subsequent N_2 and Ar exsolution. They correlated the model results to their field data, collected in pristine Dutch and Belgian aquifers, to determine the total historical organic C decomposition required to account for the observed dissolved gas concentrations. While the use of non-reactive gases (i.e., Ar and N_2) to investigate physical and chemical processes occurring within aquifers has been demonstrated in various settings, to the authors' knowledge this method has not been applied within PRB systems.

The present study was conducted at the Nickel Rim Organic Carbon PRB site near Sudbury, Ontario, which was designed to treat acid mine drainage (Benner et al., 1997, 1999, 2000, 2002; Waybrant et al., 1998, 2002). As groundwater high in SO_4 and Fe(II) enters the organic carbon PRB, microbially mediated reduction of SO_4 occurs (Benner et al., 1997):

$$SO_4^{2-} + 2CH_2O + 2H^+ \rightarrow H_2S + 2CO_{2(g)} + 2H_2O \quad (1)$$

and Fe(II) then rapidly reacts with sulfide to form metal sulfides within the barrier (Benner et al., 1997):

$$Fe^{2+} + H_2S \rightarrow FeS_{(s)} + 2H^+ \quad (2)$$

Another naturally occurring reaction within the barrier, though not a part of the treatment process, is the decomposition of organic carbon coupled with methanogenesis (Stumm and Morgan, 1996):

$$2CH_2O \rightarrow CO_{2(g)} + CH_{4(g)} \quad (3)$$

Both Eqs. (1) and (3) lead to the consumption of organic C treatment material, and the production of gases.

If gas production is significant, it may induce degassing and possibly ebullition, which is defined as the vertical transport of gas bubbles driven by buoyancy forces (e.g. Amos and Mayer, 2006), and may also affect dissolved gas composition (Fig. 1). In Fig. 1a, initial anoxic groundwater is shown, with N_2 and Ar at atmospheric levels, and slightly elevated CO_2. Fig. 1b shows that CO_2, CH_4, and H_2S gases are being produced, as a result of SO_4 reduction and methanogenesis, thus increasing the total gas pressure in the system. In Fig. 1c, a critical pressure threshold is reached, considered here to be the hydrostatic pressure, causing a gas bubble to form. Dissolved gases partition into the gas phase, and this process will lead to the depletion of the non-reactive gases Ar and N_2. In Fig. 1d, the gas bubble is mobilized, which may occur if the bubble reaches a critical size and buoyancy forces overcome capillary forces. Bubble transport may lead to ebullition and the removal of the bubble from the system.

The specific objectives of this work include the use of dissolved gas analysis to determine the ratio between SO_4 reduction and methanogenesis, and thus organic C consumption that can be attributed to each process, to delineate the rates of SO_4 reduction and methanogenesis, and to assess if gas composition can be used as a proxy for residence time to provide additional information on the existence of slow and fast flow zones within the PRB. A 4-gas degassing model (Amos et al., 2005) was used to determine the ratio between dominant terminal electron accepting processes (TEAP's) occurring within the PRB, and reactive transport simulations were conducted to assess the suitability of a simple equilibrium-based degassing model to describe the process of gas exsolution at this site.

2. Site description

The current study was conducted at the organic carbon PRB near the Nickel Rim mine site, in

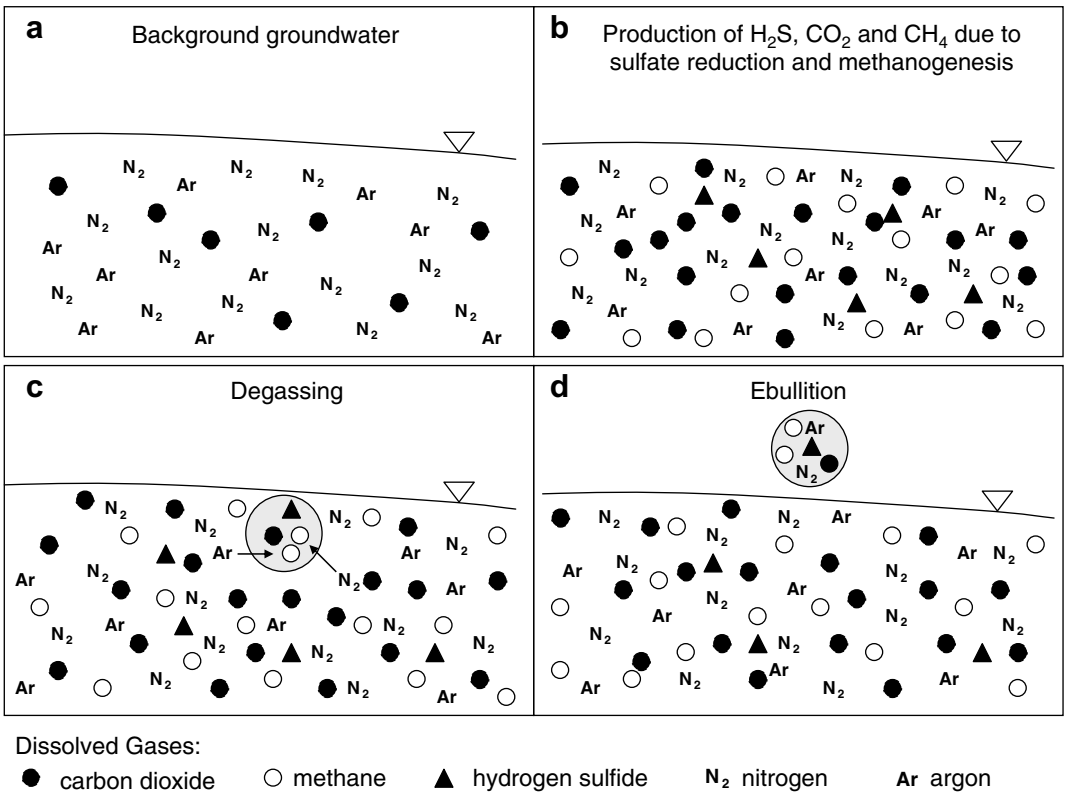

Fig. 1. Conceptual diagram of: (a) typical groundwater, high in atmospheric gases; (b) gas production (i.e., increasing CO_2 and CH_4) resulting from SO_4 reduction and methanogenesis; (c) gas accumulation and degassing of all gases in groundwater; and (d) ebullition. Assuming no other sources of Ar or N_2 concentrations in groundwater, both (c) and (d) result in depletion of the atmospheric gases N_2 and Ar.

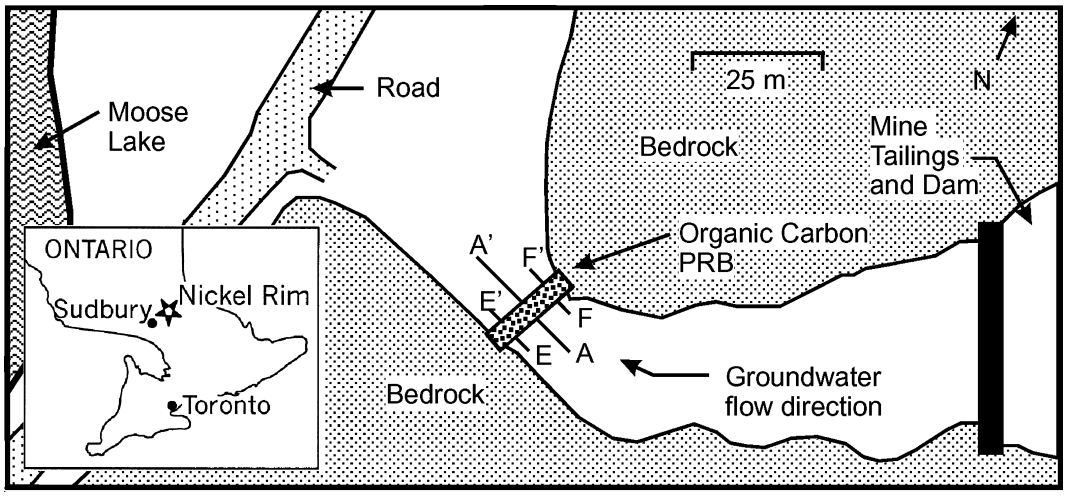

Fig. 2. Map view of the Nickel Rim PRB installation showing the mine tailings impoundment, groundwater flow path, and the location of the reactive barrier and monitoring well transects. After Benner et al. (1997).

Sudbury, Ontario (Fig. 2, after Benner et al., 2002). The hydrogeology of the site has been well characterized by Johnson (1993), Bain et al. (1995), and Bain (1996). The installation of the PRB took place in August 1995 (Benner et al., 1997). Contaminant treatment, geochemistry, microbiology and flow processes within the PRB, are described in Benner et al. (1997, 1999, 2000, 2002), Herbert et al. (2000) and Doerr et al. (2005).

Groundwater originating from the tailings impoundment follows two paths ending at Moose Lake. Approximately half of the water originating from the tailings impoundment flows within the alluvial aquifer, passing through the PRB. The remaining water seeps out at the base of the tailings dam and reaches Moose Lake as surface water (Benner et al., 1997). The groundwater plume is high in Fe and SO_4 concentrations (500–2000 mg L^{-1} Fe and 1000–7000 mg L^{-1} SO_4) and is slightly acidic (pH 4–6) (Bain, 1996). The aquifer is bounded by bedrock to the north, south, and base, and groundwater velocities are estimated to be 16 m a^{-1}. Monitoring points have been installed along three transects passing through the PRB, A–A′, E–E′, and F–F′, as shown in Fig. 2.

3. Methods

Barrier monitoring points within nests RW29, RW30, and RW31 are 3.2 cm (11/4 in.) multi-level wells and all other points are 0.6 cm (1/4 in.) bundle piezometers (Fig. 3). At least three well volumes were purged at low flow rates (25–200 mL min^{-1}) prior to sample collection at the well points, and

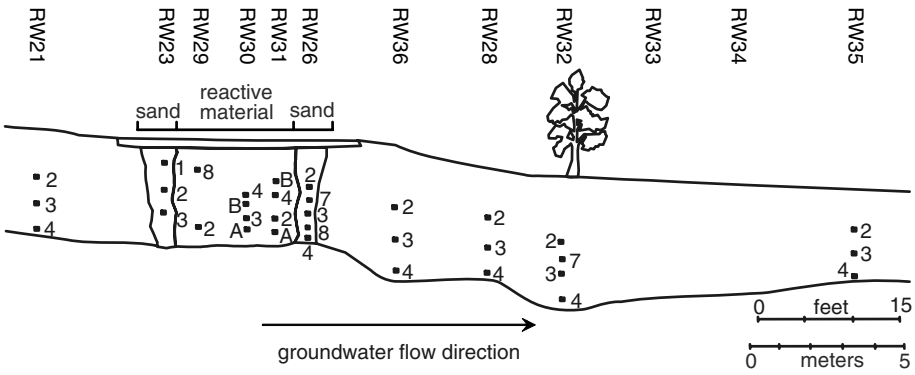

Fig. 3. Sampling locations at the Nickel Rim PRB for July 2003 along cross-section A–A′. Labels at the monitoring points define the various ports of each multilevel well (e.g. RW21-2). The vertical scale is consistent with the horizontal scale. After Benner et al. (1999).

sample collection flasks were purged with at least 10 flask volumes.

Peristaltic pumps were the chosen method of groundwater extraction at this site, due to the small tubing diameter of the bundle piezometers and monitoring wells. The dissolved gas data did not seem jeopardized by using peristaltic pumps, due to the shallow depth of the water table at the site (approximately 0.5 m) and the low pumping rates used. Bubbles were not observed in the line while pumping.

3.1. Analytical methods

Dissolved gas sampling of monitoring points in well nests along transect A–A′ (Figs. 2 and 3) took place during July 2003. All samples were analyzed in the field for dissolved CH_4, CO_2, Ar, N_2, O_2, H_2 and H_2S gases using a Varian Micro CP-4900 portable gas chromatograph (GC). Determinations of pH (Fisher Scientific Accumet AP25 meter and Orion refillable probe) were made at each piezometer. The pH probe was calibrated and regularly checked using pH 4.0 and pH 7.0 buffer solutions. Dissolved O_2 was also analyzed using CHEMets colorimetric field kits (0–1 mg L^{-1}, 1–10 mg L^{-1}) (CHEMets, Inc., Calverton, Va), and H_2S was analyzed using CHEMets sulfide field kits (0–1 mg L^{-1}, 1–10 mg L^{-1}, with activation solution A-9500) (CHEMets, Inc., Calverton, VA). Ebullition of gas bubbles was visible above the PRB in standing water at the site after rain events. The emanating gas was collected in flasks, and triplicate samples were analyzed.

Dissolved gases were analyzed in the field using the headspace method described by Amos et al. (2005). Sampling of dissolved gas species was performed by flushing groundwater through an airtight 125 mL glass flask before sample collection. After the flask had been sufficiently flushed (greater than 10 flask volumes), 15 mL of ultra high purity (UHP) He gas was added to the flask as equal parts of the sample were removed, and the sample was agitated for 10 min to allow equilibration with the headspace. A 10 mL gas sample was then removed from the headspace and the sample was analyzed on the GC. The GC was calibrated each day in the field using a single-point calibration gas (Sigma–Aldrich 5% CO_2, CO, N_2 and O_2; 4% H_2, CH_4 and He), air, and 3% H_2S gas. The accuracy of the headspace technique was evaluated using six analyses of water samples equilibrated with the atmosphere (WEA) and seven duplicate field samples. For the WEA analyses, the standard deviation was less than 5% for all gases present at significant concentrations (Ar, O_2 and N_2). The average variation between the duplicates normalized to the mean concentrations of each gas was 13.6% (CH_4), 6.7% (CO_2), 21% (Ar) and 11.0% (N_2). These variations are small in comparison to the large changes in dissolved gas composition along the flowpath.

3.2. 4-Gas analytical model

A 4-gas degassing model considering N_2, Ar, CO_2 and CH_4 was developed based on the governing equations by Cirpka and Kitanidis (2001), and is described by Amos et al. (2005). The groundwater at the site is anaerobic, which allowed O_2 to be disregarded in the model calculations.

Each ''step'' in the model corresponds to reaction progress, which can be correlated to residence time, but due to local variations in flow velocity not necessarily travel distance through the barrier. For each step update of the model, production of CH_4 and CO_2 increase the total pressure until a critical threshold is reached, and bubble formation and degassing occurs as shown in Fig. 1c. All gases dissolved in the water equilibrate with the bubbles according to Henry's Law (Table 1), and dissolved concentrations of the inert gases present, i.e., N_2 and Ar, therefore decrease.

Production of CO_2 due to microbially mediated reduction of SO_4 is described by Eq. (1). Increases in CO_2 and CH_4 due to methanogenesis are described by Eq. (3), implying a 1:1 ratio of CH_4 to CO_2 production by methanogenesis. The remaining CO_2 measured is assumed to be a product of

Table 1
Henry's Law constants used for 4-gas model calculations for $T = 270$ K

Gas	H_2	Ar	O_2	N_2	CH_4	H_2S	CO_2
K_H (M atm^{-1})	8.3×10^{-4}	1.6×10^{-3}	1.5×10^{-3}	7.4×10^{-4}	1.7×10^{-3}	1.2×10^{-1}	4.5×10^{-2}

All Henry's Law constants are from the CRC Handbook of Chemistry and Physics (1994), except for CH_4 values, which were taken from Yamamoto et al. (1976).

SO_4 reduction. Different ratios of SO_4 reduction to methanogenesis were used to optimize the fit to measured partial pressures at each sampling point within the PRB.

The pH measured within the barrier ranged from 6.3 to 6.9, which required including the speciation of dissolved CO_2 into HCO_3^- into the 4-gas degassing model using the equation (Stumm and Morgan, 1996):

$$CO_{2(aq)} + H_2O \leftrightarrow H^+ + HCO_3^-$$
$$\log K_1 = -6.40 \text{ for } T = 17\,^{\circ}C \quad (4)$$

where T is temperature and K_1 is the equilibrium constant for the reaction, respectively. Model calculations were based on a groundwater temperature of 17 °C (290 K), which is consistent with temperature values reported by Benner et al. (2002) for mid-July, which coincides with the time of sampling. Groundwater temperatures within the aquifer and barrier exhibit large seasonal variations, with an annual variation of 17 °C (Benner et al., 2002). Model calculations for July do not, therefore, represent annual barrier performance.

The 4-gas model assumes an initial amount of SO_4, based on observed concentrations up gradient of the barrier (20–40 mmol L^{-1}). Sulfate reduction is initially assumed to be independent of SO_4 concentrations, but the SO_4 reaction rates decrease for low SO_4 concentrations (Benner et al., 2002), suggesting that a Monod-type expression is suitable. Therefore, for the 4-gas model, a new ratio of SO_4 reduction to methanogenesis is calculated within the model as the initial SO_4 concentration declines. The new ratio (R_{new}) is calculated as a fraction of the initial ratio (R_{int}) using the expression

$$R_{new} = R_{int} \cdot \left(\frac{[SO_4]}{K_{SO_4} + [SO_4]} \right) \quad (5)$$

where $[SO_4]$ is the total concentration of dissolved SO_4 [mol L^{-1}] and the half saturation constant (K_{SO_4}) equals 1.62×10^{-3} mol L^{-1} based on literature data (Boudreau and Westrich, 1984; Roychoudhury et al., 1998).

Chloride data and flow modeling based on boundary and initial conditions from Benner et al. (2002) were used to estimate residence times for the points sampled within the barrier. These residence times were used in conjunction with mass of SO_4 reduced at each data point using the 4-gas model, which allowed the estimation of SO_4 reduction rates.

3.3. Reactive transport modeling

Reactive transport modeling was conducted using MIN3P (Mayer et al., 2002) based on a chemical and physical framework nearly identical to that described in Mayer et al. (2006), who conducted model simulations of the Nickel Rim PRB over a 3.5-a time period. Here, methanogenesis was included to facilitate the simulation of degassing and the modeling period was extended over 8 a of barrier operation. For details on the modeling setup not described in the following sections (model description, chemical reaction network, boundary and initial conditions, method to account for the influence of seasonal temperature variations, etc.), refer to Mayer et al. (2006).

A multi-modal Monod-type rate expression was used to simulate the observed long-term decline in barrier reactivity and rate dependence on SO_4 concentration (Mayer et al., 2006). The rate expression is defined as:

$$R_{SO_4-H_2S} = -\sum_{i=1}^{N_{org}} k_{i,SO_4-H_2S} \left(\frac{[SO_4]}{K_{SO_4} + [SO_4]} \right) \quad (6)$$

where N_{org} is the number of organic C fractions with different reactivity and k_{i,SO_4-H_2S} is the effective rate coefficient for fraction i (mol dm^{-3} s^{-1}). The half saturation constant (K_{SO_4}) is consistent with that used in the 4-gas analytical model. Methanogenesis was described by the following reaction:

$$CH_2O + \frac{1}{2}H_2O \rightarrow \frac{1}{2}CH_{4(aq)} + \frac{1}{2}CO_3^{2-} + H^+ \quad (7)$$

Due to the lack of information on reaction intermediates, the fermentation of organic C and the consumption of the fermentation products by SO_4 reduction and by methanogenesis are described as overall reactions. Mayer et al. (2006) used three organic C fractions to describe the reactivity loss in the system over a time of 3.5 a. For the 8-a investigated here, the number of organic C fractions was extended to $N_{org} = 4$, representing fractions of decreasing reactivity (with fraction 1 being the fastest and fraction 4 being the slowest to react).

Degassing of Ar, CH_4, CO_2 and N_2 was included in the simulations to investigate if gas exsolution can reproduce field-measured concentrations of these gases. The equation incorporated into the MIN3P code used to calculate the degassing rate is (Mayer et al., 2001):

$$R_d = k_d \max\left[\left(\frac{\sum_{i=1}^{Ng} p_i^g}{p_a + 9.869\times10^{-6}\rho_w g(h_i - z_i)} - 1\right), 0\right] \quad (8)$$

where k_d defines the rate coefficient of the degassing reaction (5×10^{-9} mol L^{-1} H_2O s^{-1}, calibrated), g the gravitational acceleration (m s^{-2}), p_a is the atmospheric pressure (atm), and ρ_w is the density of water (kg m^{-3}). The confining pressure is calculated on the basis of the nodal hydraulic head obtained from the flow solution (h_i(m) and the elevation head z_i(m)). Calibration of the degassing rate led to a simulation in which the first term in the brackets of Eq. (8) is close to zero, representative of equilibrium conditions. Henry's Law equilibrium constants were updated as a function of temperature via the Van't Hoff Equation. The transport of gas bubbles was not considered; it was assumed that gas bubbles leave the saturated zone instantaneously and exit to the atmosphere.

4. Results and discussion

4.1. Dissolved gases and water chemistry

Dissolved gas results show that Ar and N_2 are generally depleted within the Nickel Rim PRB, relative to groundwater up gradient of the barrier (Fig. 4), indicating that degassing is taking place. Depletion of Ar and N_2 was also seen down gradient of the PRB (Fig. 4), though the depletion was less than that seen within the top and base of the PRB. The depletion of Ar and N_2 within the PRB correlates well with an increase in concentrations of dissolved CH_4 (2.13–21.61 mg L^{-1}, or 0.07–0.73 atm) and CO_2 (301.00–831.89 mg L^{-1}, or 0.15–0.40 atm) relative to up gradient CH_4 (0.03–0.08 mg L^{-1}, or 0.001–0.003 atm) and CO_2 concentrations (136.77–197.20 mg L^{-1}, or 0.07–0.10 atm), and less elevated concentrations of CH_4 (1.39–15.37 mg L^{-1}, or 0.05–0.61 atm) and CO_2 (255.27–722.59 mg L^{-1}, or 0.13–0.36 atm) down gradient of the PRB. Within the PRB, the greater depletion of Ar and N_2 in the top and bottom portions of the barrier relates well with the more elevated concentrations of dissolved CH_4 and CO_2 at these locations. Overall, the dissolved O_2 data (not shown) indicates that groundwater is anoxic throughout the studied area, and dissolved $H_{2(g)}$ (not shown) is below the detection limit of 1 mg L^{-1}. Hydrogen sulphide gas odours were present at several sampling locations within the barrier, but were only detected at RW30-a (12.77 mg L^{-1} or 0.003 atm), which also showed highest CH_4 concentrations and strong depletion in Ar and N_2. Complementary H_2S analysis using CHEMets kits also showed that total H_2S was not present up gradient or down gradient of the barrier. Within the barrier, dissolved H_2S was only detected at RW30-a (3 mg L^{-1}) and RW29-2 (0.1 mg L^{-1}). Field-measured pH ranged from 5.5 to 6.3 up gradient of the barrier, 6.3 to 6.9 within the barrier, and from 6.3 to 6.5 down gradient of the barrier (Williams, 2005). Observed pH-values were higher within the top and bottom portions of the barrier than in the central portion of the barrier. The pH-values down gradient of the barrier appeared to be consistent with measurements within the central portion of the barrier.

It should be noted that both observed N_2 and Ar partial pressures exceed atmospheric levels (0.73 and 0.008 atm, respectively) up gradient of the PRB (Fig. 4). The enrichment of N_2 and Ar are likely a result of O_2 depletion in the unsaturated zone of the tailings impoundment where the groundwater originates or may be partially attributed to "excess air". Though the source of elevated N_2 and Ar partial pressures is uncertain, the trend in N_2 and Ar depletion along the flow path is clear.

Ebullition of gas bubbles was observed above the barrier in a pool of water that had accumulated at the site after rain events. The location of the barrier where ebullition occurred appeared to be an imperfection in the clay cover, likely the result of coring performed at previous sampling events. Analysis of this gas indicated that it consisted of approximately 51.7% CO_2, 24.9% CH_4, 23.0% N_2 and 0.4% Ar as mole fractions, with a rate of ebullition from this location estimated to be 42 L day^{-1}, based on triplicate measurements. This observation confirms that degassing and ebullition is taking place at the Nickel Rim site.

Fig. 4 shows that concentrations of CH_4 and CO_2 continue to be elevated down gradient of the barrier, while N_2 and Ar remain depleted. Concentrations of dissolved gases within the groundwater down gradient of the barrier are most similar to groundwater exiting the barrier along the faster flow paths. Because the pore water down gradient of the barrier has attained a gas composition similar to the composition within the barrier, it appears that little physical mixing of treated and untreated groundwater is occurring, and that the pore water composi-

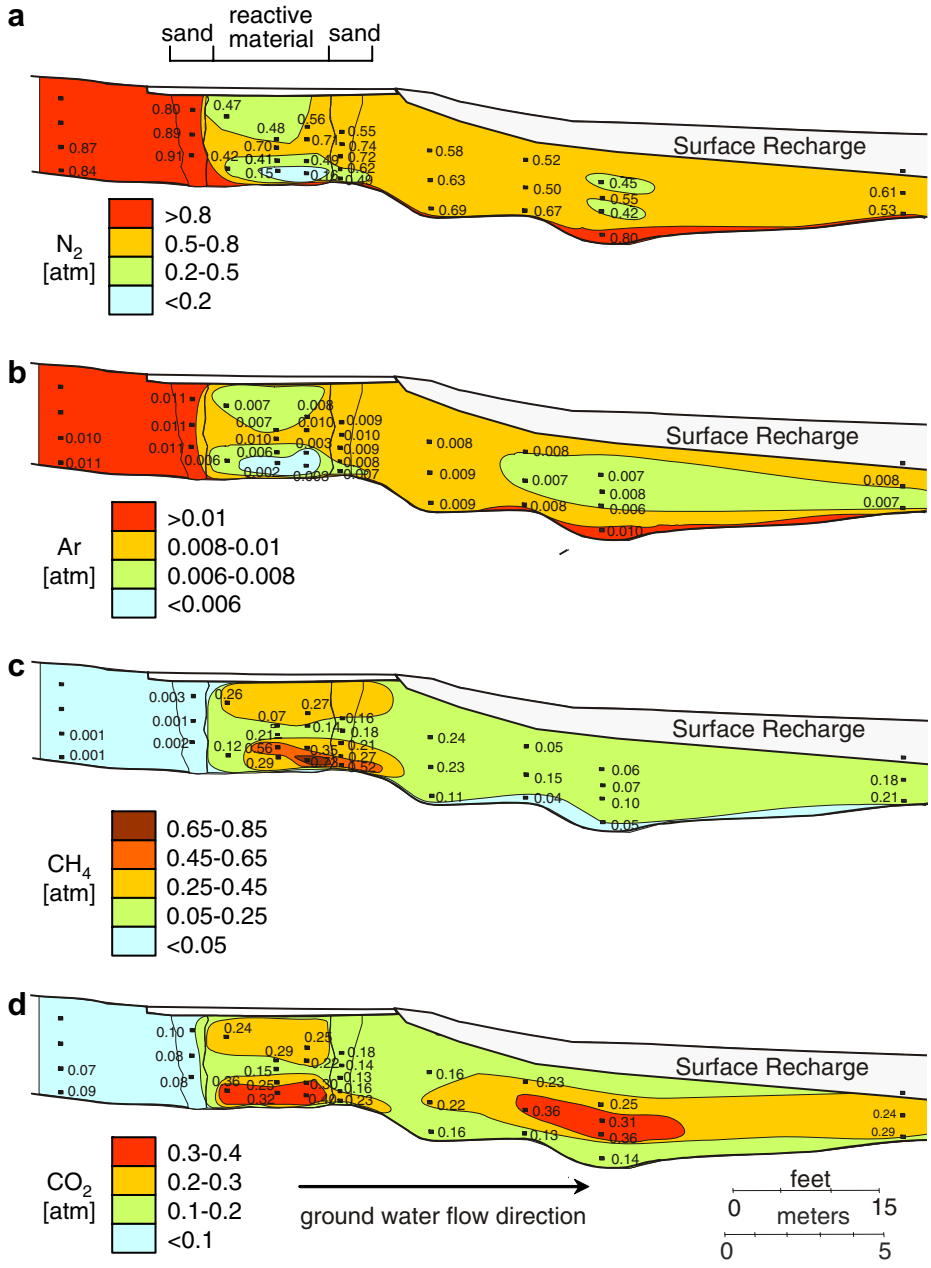

Fig. 4. Observed gas partial pressure contours (atm) in the Nickel Rim PRB study area for July 2003: (a) N_2, (b) Ar, (c) CH_4, and (d) CO_2.

tion in Ar and N_2 depleted zones is representative of the composition of treated water.

4.2. Ratio between sulfate reduction and methanogenesis

The 4-gas analytical model (Amos et al., 2005) was used to reproduce observed dissolved N_2, Ar, CH_4 and CO_2 at each location sampled within the barrier along transect A–A′. The simulations were carried out for assumed pH-values of 6.5 to account for the effect of carbonate speciation on dissolved CO_2. Observed gas partial pressures are presented in Fig. 5 for well nest 29–31, corresponding to the portion of cross section A–A′ that is located within the PRB, and are plotted in direct comparison to the results of the 4-gas model. Observed values were fitted along the "step" axis (corresponding to reaction

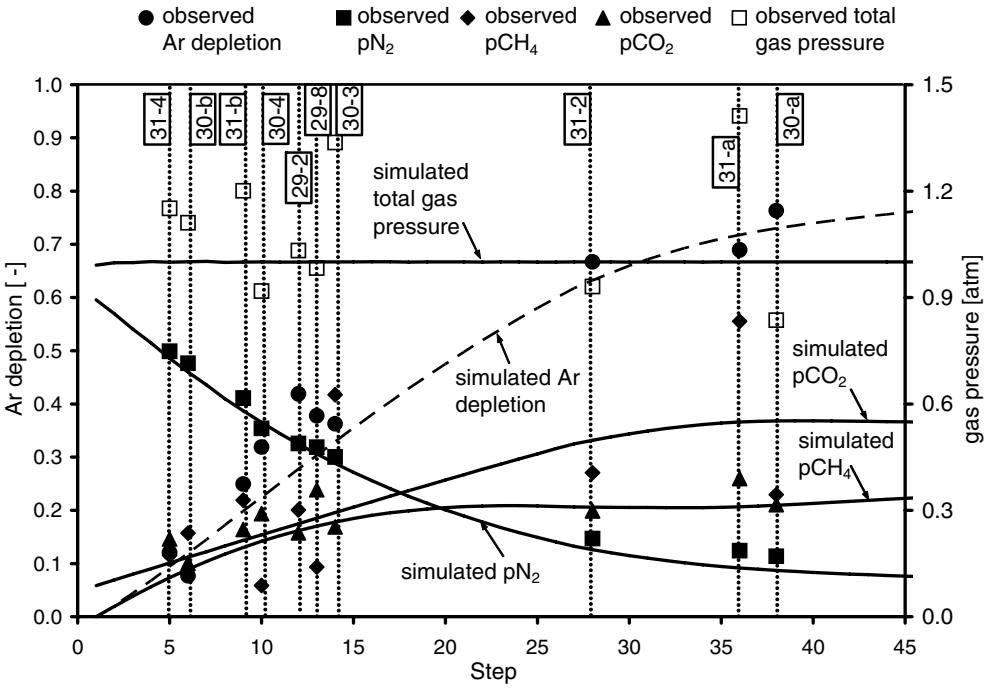

Fig. 5. 4-Gas model results plotted with observed partial and total pressure gas measurements from well nests 29, 30, and 31 along transect A–A′. A ratio of SO_4 reduction to methanogenesis of 16:1 was used in the model.

progress) until a good match for simulated N_2 and Ar was obtained, CO_2 and CH_4 were treated as dependent variables. The best overall fit was achieved using a ratio of SO_4 reduction to methanogenesis of 16:1. This ratio was determined by visual assessment of trial simulations, but appears to be a reasonable estimate, as it was also the average of the specific ratios used in simulations for individual sampling locations, as discussed below. As a result of the calibration process, N_2 and Ar average errors (not shown) are low at 3.8% and 7.2%, respectively, while CO_2 and CH_4 average errors are 25% and 50%, respectively.

Fig. 5 shows that observed gas compositions from zones of elevated CH_4 and CO_2 (29-2, 30-a, 30-3, 31-2, 31-a, as indicated in Fig. 4) are comparable with simulated data for a large number of degassing "steps" (advanced reaction progress). Simulated N_2 partial pressures are much lower than atmospheric levels and Ar depletion is greater at these sampling locations, generally corresponding well with observed data, and indicating a significant degree of degassing. Observed gas partial pressures for sampling locations with less elevated CH_4 and CO_2, and less depletion of N_2 and Ar (29-8, 30-4, 30-b, 31-4, 31-b, as indicated from Fig. 4) tend to correlate with the model results for fewer "steps" (limited reaction progress). The consistent agreement between observed and simulated gas compositions suggests that the equilibrium-based degassing model captures the process of gas exsolution driven by SO_4 reduction and methanogenesis adequately. The results also indicate that the samples from various locations have undergone a different degree of reaction progress, relatively independent from the distance of the sampling location from the up gradient end of the barrier.

Fig. 5 indicates that the ratio of 16:1 between SO_4 reduction and methanogenesis is not equally applicable for all sampling locations. For this reason, the 4-gas model was also used to match each data point individually using a sampling location specific ratio of SO_4 reduction to methanogenesis to improve the match between observed and simulated gas partial pressures. The measured total gas pressure was used as an additional constraint in these simulations. For example a lower ratio of SO_4 reduction to methanogenesis of 7:1 provides a better fit to the observed results for well 31-2 (Fig. 6). The observed data for sampling locations with a greater degree of degassing were better fit to the model using lower ratios of SO_4 reduction

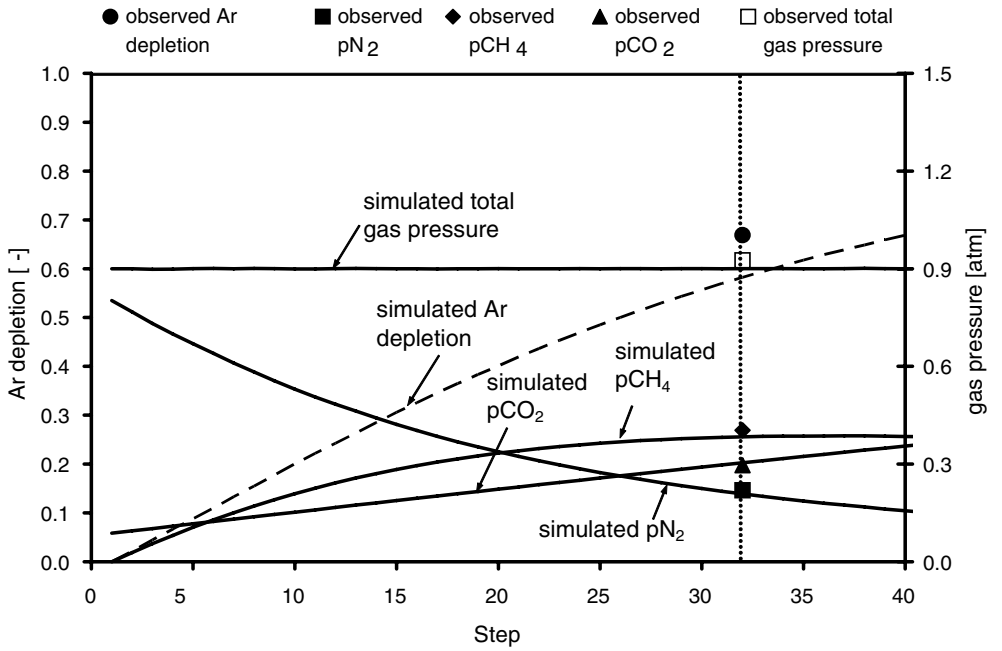

Fig. 6. 4-Gas model results plotted with observed partial and total pressure gas measurements for sampling location 31-2 along transect A–A′. A ratio of SO_4 reduction to methanogenesis of 7:1 was used in the model.

to methanogenesis than for sampling locations with a lower degree of degassing, indicating that more organic C is consumed by methanogenesis in zones of advanced reaction progress. Table 2 summarizes the calibrated ratios of SO_4 reduction to methanogenesis for sampling locations along A–A′ within the barrier. Using this approach the average relative error (error results not shown) between observed and simulated data ranges between 5.1% and 9.3% for the various gases. The ratios for all sampling locations are greater than or equal to 5:1, indicating that the majority of the organic C throughout the barrier is being consumed by SO_4 reduction.

The average ratio of SO_4 reduction to methanogenesis in zones of advanced degassing is 8:1 (based on wells 29-2, 30-a, 30-3, 31-2, and 31-a), while the average ratio for sampling locations in zones of limited degassing was 24:1 (based on wells 29-8, 30-4,

Table 2
Ratios of SO_4 reduction to methanogenesis used to fit observed gas partial pressures at each sampling location within the barrier to the 4-gas model

Sample point	Ratio of SO_4 reduction to methanogenesis	SO_4 removed (mg L^{-1})	CH_4 produced (mg L^{-1})
29-2	15	792	8.8
29-8	40	1344	5.6
30-a	7	1243	29.6
30-4	45	864	3.2
30-3	7	907	21.6
30-b	7	269	6.4
31-2	7	974	23.2
31-a	5	1584	52.8
31-4	15	504	5.6
31-b	15	864	9.6
Greater degassing zone	8		
Limited degassing zone	24		
Overall average	16		

Resulting estimates of SO_4 removal and CH_4 produced, reported as mg L^{-1}, based on observed gas partial pressures at each sampling location and the 4-gas model.

30-b, 31-4, 31-b) (Table 2). Assuming an overall average ratio of SO_4 reduction to methanogenesis of 16:1 is representative of conditions throughout the barrier, and using the reaction stoichiometries defined by Eqs. (1) and (3), it can be estimated that 94% of organic C consumption can be attributed to SO_4 reduction, and 6% is consumed by methanogenesis. Using the same calculation for the zones of advanced and limited degassing estimates that 89% and 96% of the organic C is consumed by SO_4 reduction, respectively.

These calculations indicate that the dominant TEAP within the barrier is by far SO_4 reduction, consistent with other observations at the site that include decreases in SO_4 concentrations along the flowpath, S isotope data indicative of SO_4 reduction, increases in concentrations of SO_4 reducing bacteria, and precipitation of metal sulfides (Benner et al., 1999). In addition, the present results allow constraining the role of methanogenesis.

The 4-gas model does not include ebullition, which will likely lead to an overestimation of methanogenesis and SO_4 reduction. A quantitative evaluation of this error is difficult, because the fraction of gas bubbles that are subject to ebullition is unknown. However, mass balance calculations using a modified version of the 4-gas model (not shown) suggest that the role of gas bubble formation has a significantly larger effect on the gas composition than ebullition, even if a significant fraction of CH_4 is lost to ebullition (e.g. 20–50%).

4.3. Residence times, reaction rates and organic carbon consumption

The presence of zones of advanced and limited degassing suggests that reaction progress and therefore residence time of the sampled pore water differs substantially among the different sampling locations. Dissolved gas data supports the existence of preferential flow, characterized by fast and slow flow zones within the barrier, as discussed by Benner et al. (2002). Using Ar and N_2 depletion as a proxy for residence time it can be seen that low flow zones exist at the top and base of the barrier (Fig. 4) along cross-section A–A′. Hydrogen sulfide was only detected at the base of the barrier along cross section A–A′, indicating that this is an area of very slow moving pore water. These results are consistent with low concentrations of Fe and SO_4 that were previously observed along cross section A–A′ at the top and bottom of the barrier, also indicating increased residence times (Benner et al., 2002).

For each "step" of the 4-gas model, SO_4 reduction can be estimated by assuming that for every 2 mol of CO_2 produced as defined by Eq. (1), 1 mol of SO_4 is reduced. More importantly, CH_4 production can be more accurately estimated using this method, because CH_4 lost to degassing is considered in the 4-gas model, which is not the case when deriving rates from dissolved CH_4 concentrations only. The results for estimated SO_4 reduction and CH_4 production at each sampling location are shown in Table 2.

The 4-gas model is based on equilibrium batch reactions, and time is not included in the model. Estimation of rates of SO_4 reduction and methanogenesis requires that residence times from the barrier entry to each specific sampling point are known. These residence times were determined using Visual MODFLOW (Guiguer and Franz, 1997) flow and particle-tracking simulations, based on flow modeling for the PRB by Benner et al. (2002). Rates were determined using the equation:

$$\text{Rate} = \frac{\Delta C}{t_r} \tag{9}$$

where ΔC is the change in SO_4 or CH_4 concentration from the barrier influent to each sampling location, as shown in Table 2, and t_r is the residence time from the barrier entry to the barrier sampling point, estimated from flow modeling results. Table 3 lists t_r and the estimated rate for each sample location, and in addition provides estimated residence times through the entire barrier along the flow paths which pass through the specific sample locations. These residence times further confirm that zones of greater degassing (i.e., greater Ar or N_2 depletion), fall into the slower flow path regime, while zones of limited degassing fall into the fast flow path regime. The SO_4 reduction and removal rates determined using this method compare well with the results of Benner et al. (2002) and Herbert et al. (2000), and a comparison is presented in Table 4. However, the main advantage of the current method is its capability to provide an estimate of methanogenesis rates. This is not possible using methods that neglect the role of degassing. Estimated methanogenesis rates vary between 1.7 and 10.1 mmol L^{-1} a^{-1} (27–161 mg L^{-1} a^{-1}) and average at 5.1 mmol L^{-1} a^{-1} (80 mg L^{-1} a^{-1}) for the entire barrier.

Table 3
Residence times, SO_4 reduction and methanogenesis rates based on MODFLOW flow and particle tracking simulations and 4-gas model results

Sample point	Ratio of SO_4 reduction to methanogenesis	Estimated residence time through PRB and point (days)	Estimated residence time from entry to sample point (days)	Methanogenesis rate (mmol L^{-1} a^{-1})	SO_4 reduction rate (mmol L^{-1} a^{-1})
29-2	15	132	20	10.1	151
29-8	40	73	13	9.9	393
30-a	7	548	250	2.8	19
30-4	45	72	42	1.7	78
30-3	7	128	78	6.4	44
30-b	7	72	42	3.5	24
31-2	7	126	108	5.0	34
31-a	5	226	190	6.5	32
31-4	15	74	62	2.1	31
31-b	15	74	62	3.6	53
Slow path average	8	232		6.1	56
Fast path average	24	73		4.2	116
Average	16	153		5.1	86

Table 4
Comparison of removal estimates using the 4-gas degassing model with estimates derived from previous studies

	Residence time (days)	SO_4 reduced (mmol L^{-1} pv^{-1})	Rate of SO_4 reduction (mmol L^{-1} a^{-1})
Current work[a] *flow path*			
Slow	232	26	56
Fast	73	23	116
Average	153	25	86
Benner et al. (2002)[b] *flow path*			
Slow	160	31	71
Fast	60	5	30
Average	90	13	53
Herbert et al. (2000)[c] flow path			
Slow			25
Fast			36
Average			

[a] Calculations for current work are based on observed gas data fit to the 4-gas analytical model.
[b] Benner et al. (2002) calculations are based on changes in aqueous concentrations (influent–effluent).
[c] Herbert et al. (2000) calculations are based on solid phase digestions, converted to aqueous concentrations in Benner et al. (2002).

Due to the many uncertainties, a detailed comparison between SO_4 removal estimates shown in Table 4 is not warranted. The estimates by Benner et al. (2002) were developed based on the lowest influent SO_4 concentrations and the highest effluent concentrations, and as a result probably indicate the low end of the rate scale. Herbert et al. (2000) estimates are based on solid phase digestion data for a 23 month period, converted to aqueous concentrations. Previous estimates by Benner et al. (2002) were based on seasonal averages, while rates for the current work are for summer conditions, which are more conducive for microbial activity. Benner et al. (2002) determined that seasonal temperature fluctuations cause large variations in SO_4 removal rates. Because removal rates for this study are determined for locations within the barrier, they could potentially be higher than estimates based on influent–effluent data.

The gas data also allows for a crude present-day estimate of treatment material (defined as CH_2O) consumption. The amount of CO_2 and CH_4 produced in moles per litre of groundwater within the barrier can be estimated, by averaging the results of the 4-gas model simulation at each sampling location. Using Eqs. (1) and (3), this estimate can be converted to CH_2O consumed. Assuming a porosity of 0.4 within the barrier, a groundwater velocity of

16 m a^{-1}, and a cross-sectional area of 45 m^2, the groundwater flux through the barrier is 288 m^3 a^{-1} (Benner, 1999). Assuming this flux through the barrier, the annual consumption of CH_2O is 15,900 mol a^{-1}. This corresponds to a production of roughly 14,700 mol a^{-1} of CO_2 and 560 mol a^{-1} of CH_4. The barrier contains approximately 1,500,000 moles of C (Benner, 1999), and assuming that at the time of barrier installation 10% of the carbon (approximately 150,000 moles) was reactive, the barrier would be active for 9.4 a at this rate of organic C consumption. However, the reliability of this estimate is limited due to the unknown fraction of reactive organic material, the decrease in reactivity of organic matter with time (Westrich and Berner, 1984), and seasonal variations in reaction rates.

4.4. Implications of degassing and ebullition on PRB mass balance

Benner et al. (2002) suggested that H_2S degassing may be an important sink for sulfide, and could possibly account for the sulfide mass balance issue presented. The current work demonstrated that observed H_2S concentrations were low or below detection and no H_2S ebullition occurs, which suggests that degassing and ebullition are unlikely sinks for sulfide at the present time, but does not preclude that these processes did take place earlier during the barrier life when SO_4 reduction rates were faster (Benner et al., 2002). This result indicates that currently S is almost exclusively removed by precipitation reactions within the PRB, therefore providing the intended sink for Fe(II).

Although ebullition of other gases was observed only at a single point above the barrier, it is likely to occur at other locations as well. The significance of this process is unknown, but ebullition may need to be considered to accurately complete the mass balance within a PRB. To assess the potential importance of ebullition, the gas production estimate from the entire barrier can be compared to ebullition seen at the location above the barrier. Assuming the ideal gas law:

$$pV = nRT \tag{10}$$

can be applied to the ebullition data described in the previous section, where p is the atmospheric pressure of 1 atm, V is the ebullition volume estimate of 42 L day^{-1}, R is the gas constant (8.206×10^{-5} m^3 atm K^{-1} mol^{-1}), T is temperature in degrees Kelvin (290°) and n are the moles of gas, where n can be estimated as the mass loss due to ebullition per year. Using these parameter values, n is estimated to be 642 mol a^{-1}, which converts to approximate losses of 160 mol a^{-1} of CH_4, 332 mol a^{-1} of CO_2, 154 mol a^{-1} of N_2, and 2 mol a^{-1} of Ar from the barrier using the mole fractions observed in the ebullition sample. It can be expected that rates of ebullition vary seasonally and diurnally and that ebullition is not restricted to a single location. Though there are a number of uncertainties in the ebullition estimates, these results do indicate that ebullition from the barrier may be sizable relative to overall gas production and may need to be considered to accurately complete the mass balance within a PRB.

4.5. Reactive transport modeling

Both pore water (Benner et al., 2002) and solid phase data (Herbert et al., 2000) after 23 months of barrier operation were used to quantitatively compare model results to field observations (Mayer et al., 2006). In this study, additional pore water data for several dates exceeding 23 months of operation, and solid phase S data (Daignault, 2002) collected after 71 months (nearly 6 a) of operation were used to calibrate the model (Williams, 2005). This data set together with the dissolved gas data collected for the current work in July 2003 allowed the consideration of methanogenesis and degassing in the simulations.

Table 5 provides a summary of the calibrated organic C fractions and reaction parameters. For SO_4 reduction, two parallel reaction pathways have been used consistent with field observations of solid phase S accumulation both as sulfides and elemental S (Herbert et al., 2000) and previous reactive transport modeling (Mayer et al., 2006). In addition to reporting rate coefficients normalized to the bulk volume of the treatment material, effective rate coefficients normalized to the organic C fractions are also provided to highlight the range of reactivity.

The most recent and complete data set for observed concentrations of SO_4, Fe, alkalinity, and pH was collected after 6 a of barrier operation, and is used in this discussion for comparison. Simulated SO_4 concentrations decline to less than 2.4×10^{-2} mol L^{-1}, while the maximum observed concentration at the down gradient end of the barrier was 2.9×10^{-2} mol L^{-1} (Fig. 7). Simulated Fe concentrations decrease to $<4 \times 10^{-3}$ mol L^{-1}, while observed concentrations do not exceed 1×10^{-2} mol L^{-1}

Table 5
Initial volume fractions and calibrated effective rate coefficients for organic C consumption reactions

Reaction	Initial volume fraction	Effective rate coefficient (mol dm^{-3} s^{-1})[a]	Effective rate coefficient (mol dm^{-3} s^{-1})[b]
CH_2O–H_2S (fast)[c]	0.0012	1.8×10^{-9}	1.5×10^{-6}
CH_2O–S (fast)[d]		5.4×10^{-10}	4.5×10^{-7}
CH_2O–CH_4 (fast)[e]		1.2×10^{-10}	9.8×10^{-8}
CH_2O–H_2S (int.)[c]	0.0015	1.3×10^{-9}	8.5×10^{-7}
CH_2O–S (int.)[d]		3.8×10^{-10}	2.6×10^{-7}
CH_2O–CH_4 (int.)[e]		8.3×10^{11}	5.5×10^{-8}
CH_2O–H_2S (slow)[c]	0.0018	9.3×10^{-10}	5.2×10^{-7}
CH_2O–S (slow)[d]		2.8×10^{-10}	1.5×10^{-7}
CH_2O–CH_4 (slow)[e]		6.0×10^{-11}	3.4×10^{-8}
CH_2O–H_2S (slowest)[c]	0.3290	1.0×10^{-9}	3.0×10^{-9}
CH_2O–S (slowest)[d]		3.0×10^{-10}	9.1×10^{-10}
CH_2O–CH_4 (slowest)[e]		6.5×10^{-11}	2.0×10^{-10}

[a] Normalized to bulk volume of treatment material.
[b] Normalized to volume of organic C fraction.
[c] Reaction stoichiometry: $CH_2O + \frac{1}{2}SO_4^{2-} \rightarrow HCO_3^- + \frac{1}{2}H_2S(aq) + H_2O$.
[d] Reaction stoichiometry: $CH_2O + \frac{2}{3}SO_4^{2-} + \frac{1}{3}H^+ \rightarrow HCO_3^- + \frac{2}{3}S^0(s) + \frac{2}{3}H_2O$.
[e] Reaction stoichiometry: $CH_2O + \frac{1}{2}H_2O \rightarrow \frac{1}{2}CH_4(aq) + \frac{1}{2}CO_3^{2-} + H^+$.

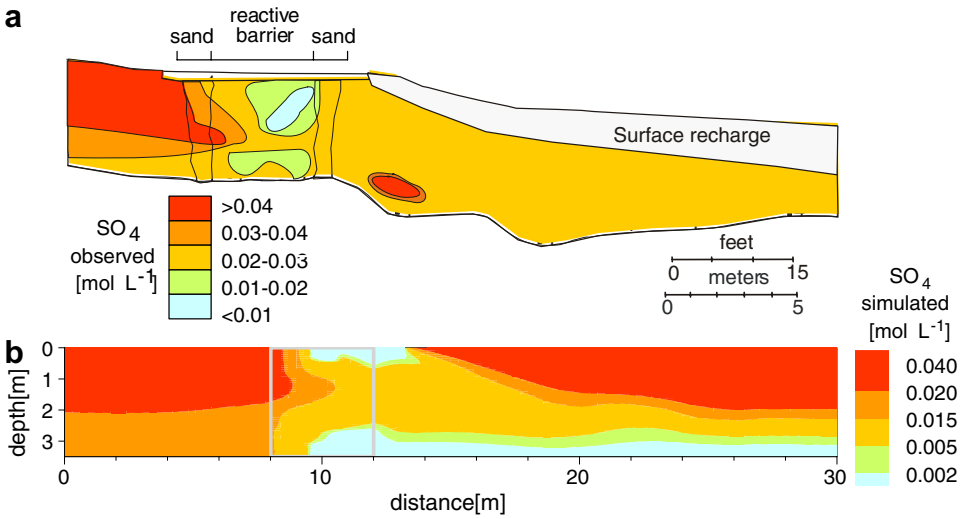

Fig. 7. SO_4 concentration contours (mol L^{-1}) after 72 months of barrier operation: (a) observed and (b) simulated.

(Williams, 2005). Generally, the modeling results achieve a good match to both the observed concentration changes and solid phase accumulation within the barrier for 6 a (Williams, 2005).

Most importantly, the simulations provide a good match to the observed gas partial pressure data for July 2003 (compare Figs. 4 and 8). The observed trends of greater CO_2 and CH_4 partial pressures in the top and bottom sections of the PRB (i.e., low flow zones) and greater Ar and N_2 depletion in these sections were reproduced. The rates of methanogenesis and degassing were calibrated until a reasonable fit to the observed gas data was found. Rates of methanogenesis of 10, 20, and 16 times less than the rate of SO_4 reduction were attempted, and similar to the findings of the 4-gas degassing model calculations presented previously, a ratio of 16:1 provided the best fit. These findings further confirm the results of the 4-gas model, which indicated that SO_4 reduction is the dominant processes leading to the consumption of organic C. Simulated CO_2 partial pressures ranged from 0.03 atm to 0.68 atm within the PRB, while the minimum and maximum observed partial pressure were 0.15 atm and 0.40 atm, respectively. Simulated CH_4 partial pressures ranged from 0.01 atm to 0.97 atm

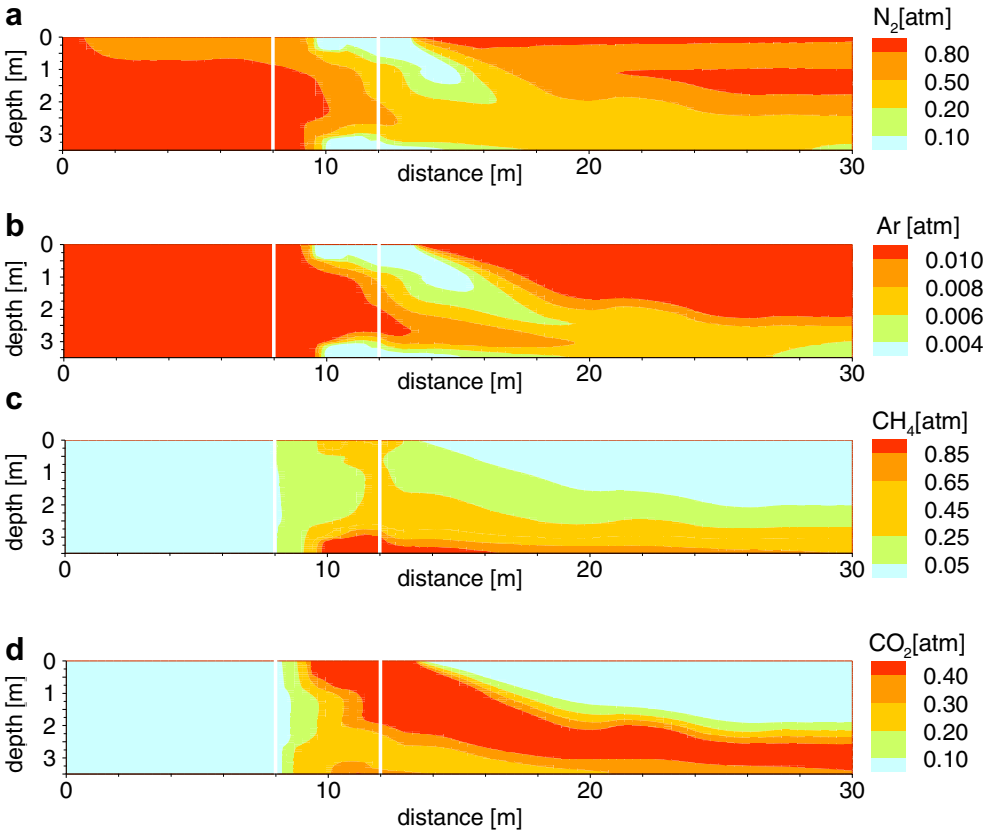

Fig. 8. Simulated gas partial pressure contours (atm) after 95 months of operation (approximately July 2003): (a) N_2, (b) Ar, (c) CH_4, and (d) CO_2.

within the PRB, while the minimum and maximum observed partial pressures were 0.07 atm and 0.73 atm, respectively. Both the observed and simulated CH_4 maximum values were found in the low flow zone at the bottom of the PRB, near the down gradient side. Down gradient of the PRB, N_2 and Ar partial pressures remain slightly depleted in both simulated and observed results, while CH_4 and CO_2 concentrations remain elevated.

Both observed, as well as simulated SO_4 reduction rates show a decrease over time (Fig. 9), and compare well with the data presented by Benner et al. (2002) and the additional data provided by Bain (unpublished). Organic C consumption due to methanogenesis was also considered, and the rate of methanogenesis mimics the trend of SO_4 reduction (Fig. 9), though at much slower rates as discussed in the previous section. Simulations show that after 95 months of barrier operation only 1.3% of the "intermediate" and 2.0% of the "slow" organic C fraction remains in the PRB. The "fast" fraction is almost entirely consumed, with only 0.6% remaining primarily in the low flow zones, which are nearly inaccessible to SO_4. The "slowest" fraction is almost untouched (>98% remain).

Degassing was considered in the model simulations, and Fig. 10 provides the degassing rates of Ar(g), CH_4(g), CO_2(g), and N_2(g) over time. Henry's Law constants for the gases of concern (Table 1) show that N_2 is the least soluble, followed by Ar and CH_4, with CO_2 being the most soluble gas. In Fig. 10, initially primarily N_2 is lost to degassing, as it is the least soluble gas and has the highest partial pressure within the groundwater. As CH_4 and CO_2 are produced and accumulate within the barrier, more of each contributes to degassing. Over time, N_2 remains the highest contributor to degassing, with equal amounts of CH_4 and CO_2 present, though in the long term all rates of degassing decrease, due to the decreasing reactivity of the treatment material. Table 6 provides a summary of the influx of total N_2(aq), Ar(aq) and TOT(CO_3), the production of CH_4(aq), and TOT(CO_3) within the barrier, and the mass of

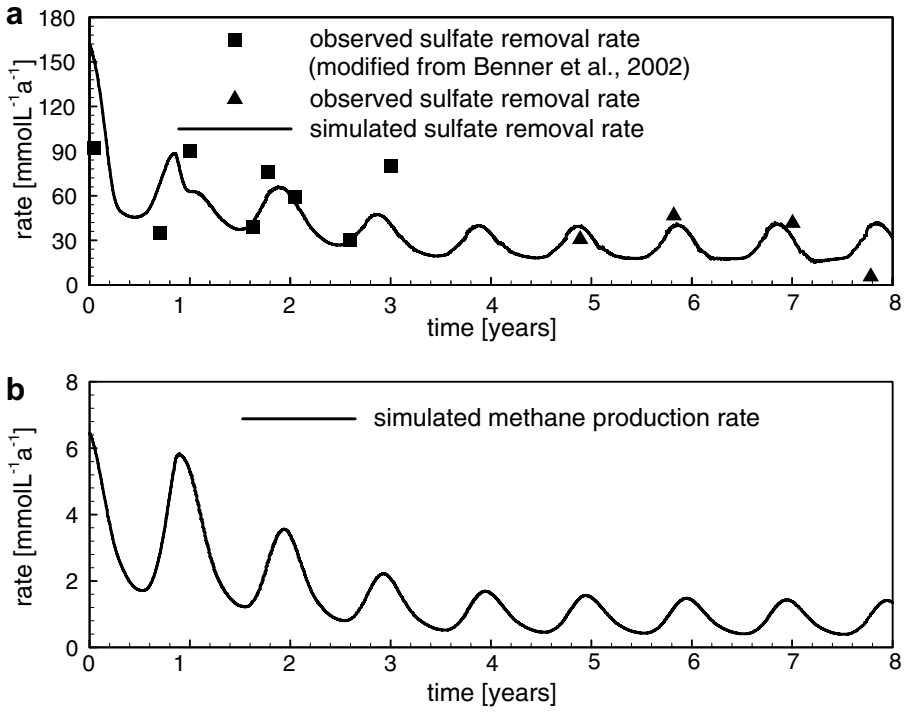

Fig. 9. Long-term trend of (a) average SO_4 reduction rates (simulated and observed) and (b) rates of methanogenesis (simulated).

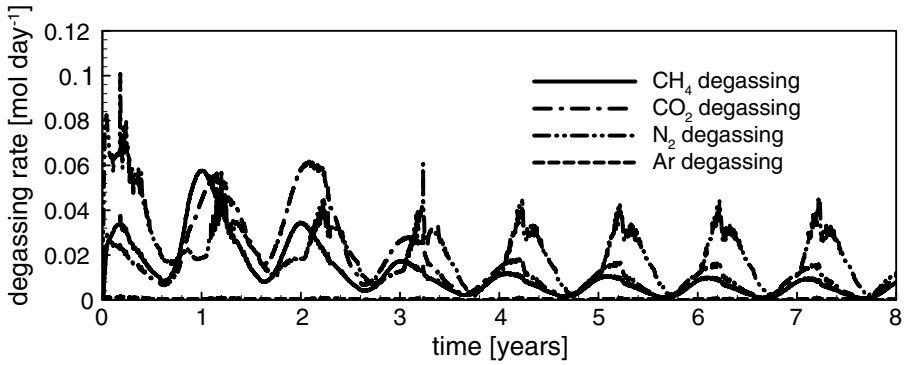

Fig. 10. Simulated degassing rates over time for CH_4, CO_2, N_2, and Ar (mol day^{-1}).

Table 6
Simulated mass balance of CH_4, TOT(CO_3), N_2, and Ar(aq) for 8 a of barrier operation estimated for the entire 15 m width of the PRB, and the resulting degassing from the barrier

Parameter	Total influx (moles)	Produced by degradation (moles)	Lost to degassing (moles)	Percent lost to degassing (%)
CH_4	0	1033	527	51
CO_3	3434	46,421	704	1.4
N_2	1983	0	914	46
Ar	55	0	17	30

each component lost to degassing over time for the 15 m wide barrier. The simulations indicate that 1033 mol of CH_4 are produced within the barrier over 8 a, and 51% of that CH_4 is lost to degassing, while only 1.4% of TOT(CO_3) is lost to degassing. This result further confirms that degassing must be

considered to properly assess the rate of methanogenesis in this system.

The current formulation of degassing assumes that gas bubbles leave the saturated zone instantaneously and exit to the atmosphere, but in all likelihood only a portion of the gas bubbles are lost to ebullition, while some gas remains trapped within the barrier. By using the ideal gas law, one can speculate about the potential importance of ebullition in respect to completing the mass balance. By assuming an average pressure, P, over depth of 1.18 atm, an average annual temperature, T, of 283 K, and an average of $n = 270$ mol a^{-1} lost to degassing (sum moles lost to degassing averaged over 8 a, Table 6), one can estimate that gas bubbles with a total volume, V, of 5.3 m^3 would form within the barrier over the period of one year. Within this time, the gas bubbles would occupy approximately 6.4% of the pore space, or reduce porosity from 0.4 to 0.37. If one assumed that all bubbles remained within the pores, and made the same calculation for the simulated 8-a period (2160 mol), a volume of 42.7 m^3 would be occupied by bubbles, which would take up 50% of the pore space. It is unlikely that this is the case, again suggesting that ebullition from the barrier is occurring. Porosity loss within the barrier due to degassing is likely occurring as well, though ebullition appears to be relieving some of that loss.

The 4-gas degassing model considers a 1 L batch system, and follows a "parcel" of pore water on a specific flow path as it passes through the barrier, but cannot account for mixing within the porous media. MIN3P, on the other hand, considers the dynamic interaction of transport and temperature-dependent reaction processes that are occurring in the PRB. When degassing occurs, MIN3P simply disposes of the volume of gas, which will lead to an underestimation of calibrated reaction rates, while the 4-gas degassing model considers that the volume of gas remains within the 1 L system, which will lead to an overestimation of the reaction rates (see above).

Estimates of CO_2 and CH_4 produced and lost to degassing were made previously using the 4-gas degassing model, based on results from specific locations within the barrier. These values can be compared to the mass balance results from the MIN3P simulations, and are summarized in Table 7. Overall, the 4-gas degassing model estimates for CO_2 and CH_4 production and CH_2O consumption within the entire barrier are factors of approximately 3–5 times higher than those obtained from the reactive transport simulations. However, the different assumptions made to obtain the estimates at least partially explain the discrepancies between the results.

In the MIN3P simulations, temporal fluctuations are considered, and therefore an average rate of CH_2O consumption over the years of operation can be calculated which takes into account slower consumption in the winter and faster consumption in the summer. The 4-gas model calculations were based on data collected during the summer of the 8th year of barrier operation, when rates of SO_4 reduction and methanogenesis are likely highest for the year, and therefore will significantly overestimate a yearly average rate. The 4-gas degassing model determined the rates of CH_2O consumption, and CH_4 and CO_2 production at specific points within the barrier, and these rates were then normalized to the entire barrier width, averaged, and assumed to be constant along the remainder of the flow path. Sulfate reduction is considered to be a Monod type reaction, indicating that again, the 4-gas model will overestimate the average rate of CH_2O consumption, because the data is representative for the sampling point within the barrier, but neglects the remainder of the flow path, where SO_4 may become limiting for the reaction process.

Both observed data and simulations (Fig. 9) indicate that rates of SO_4 reduction (i.e., the dominant consumer of CH_2O), after a rapid decline in removal during the first 2–3 a of operation, have been fairly steady for the past 5–6 a of operation. Therefore, even though the 4-gas model results

Table 7
Comparison of MIN3P and 4-gas degassing model for 8 a of treatment material consumption and annual average rates

Parameter	MIN3P simulated results		4-Gas degassing model results		4-Gas:MIN3P results
	(mol)[a]	(mol a^{-1})	(mol)[a]	(mol a^{-1})	
CH_2O consumed	44,600	5575	127,368	15,921	2.9
CO_2 produced	46,421	5803	117,576	14,697	2.5
CH_4 produced	1033	129	4512	564	4.4

[a] Indicates total moles consumed or produced after 8 a of barrier operation.

presented in Table 7 were based exclusively on data collected during the summer of the 8th year of barrier operation, it is not too surprising that by not accounting for temporal fluctuations and by normalizing rates determined at specific points within the barrier, they are higher than the reactive transport modeling results.

5. Summary and conclusions

Within the barrier, elevated CH_4 and CO_2 concentrations are observed, while N_2 and Ar concentrations are depleted in comparison to atmospheric levels. These results indicate the formation of gas bubbles within the barrier, and ebullition was indeed observed above the barrier. Hydrogen sulfide is below detection, indicating that after 8 a of operation essentially all H_2S in the barrier is removed by precipitation of metal sulfides. Observed CO_2 concentrations could be explained through production by methanogenesis and SO_4 reduction. Dissolved gas data appears to be particularly useful in providing better estimates for the rates of methanogenesis in this system.

The gas distribution within the barrier could be used as a proxy for residence times, consistent with earlier findings based on Cl and SO_4 analysis by Benner et al. (2002). On average, over 90% of the CO_2 is produced by SO_4 reduction, while the remaining CO_2 is produced by methanogenesis. While the results of the 4-gas model are not unique, and many assumptions were made in the calculations, the results indicate that SO_4 reduction is by far the main process of organic C consumption within the barrier along both the fast and slow flow paths.

Reactive transport modeling of the Nickel Rim PRB for 8 a of barrier operation generally provided a good match to observed data. Degassing was incorporated into the simulations and observed dissolved gas trends were well represented, suggesting that a simple formulation for degassing may provide a suitable description of this process, although no information on the volume change due to bubble formation or the fate of the trapped gas can be obtained.

Acknowledgements

This research was supported by the CWN (Canadian Water Network) through a grant awarded to D.W. Blowes and R. Samson (University of Montreal) and a NSERC (Natural Sciences and Engineering Research Council of Canada) Discovery Grant held by K.U. Mayer. The authors would like to thank two anonymous reviewers for their constructive comments. We also wish to thank Shawn G. Benner for his valuable comments, which helped to improve the manuscript.

References

Amos, R.T., Mayer, K.U., 2006. Investigating ebullition in a sand column using dissolved gas analysis and reactive transport modeling. Environ Sci. Technol. 40, 5361–5367.

Amos, R.T., Mayer, K.U., Bekins, B.A., Delin, G.N., Williams, R.L., 2005. Use of dissolved and vapour-phase gases to investigate methanogenic degradation of petroleum hydrocarbon contamination in the subsurface. Water Resour. Res. 41, W02001. doi:10.1029/2004WR003433.

Bain, J.G., 1996. The Physical and Chemical Hydrogeology of a Sand Aquifer Affected by Drainage from the Nickel Rim Tailings Impoundment, M.Sc. thesis, Department of Earth Sciences, Univ. Waterloo, Ontario.

Bain, J.G., Blowes, D.W., Robertson, W.D., 1995. The hydrogeochemistry of a sand aquifer affected by discharge from the Nickel Rim tailings, Sudbury, Ontario. In: Haynes, T.P., Blanchette, M.C. (Eds.), Proceedings of the Sudbury '95-Mining and the Environment. CANMET, Ottawa, pp. 715–723.

Benner, S.G., 1999. Hydrogeology, Geochemistry and Microbiology of a Reactive Barrier for Acid Mine Drainage. Ph.D thesis, Univ. Waterloo, Ontario.

Benner, S.G., Blowes, D.W., Gould, W.D., Herbert Jr., R.B., Ptacek, C.J., 1999. Geochemistry of a permeable reactive barrier for metals and acid mine drainage. Environ. Sci. Technol. 33, 2793–2799.

Benner, S.G., Blowes, D.W., Ptacek, C.J., 1997. A full-scale porous reactive wall for the prevention of acid mine drainage. Ground Water Monit. Remed. 17, 99–107.

Benner, S.G., Blowes, D.W., Ptacek, C.J., Mayer, K.U., 2002. Rates of sulfate reduction and metal sulfide precipitation in a permeable reactive barrier. Appl. Geochem. 17, 301–320.

Benner, S.G., Gould, W.D., Blowes, D.W., 2000. Microbial populations associated with the generation and treatment of acid mine drainage. Chem. Geol. 169, 435–448.

Blicher-Mathiesen, G., McCarty, G.W., Nielsen, L.P., 1998. Denitrification and degassing in groundwater estimated from dissolved dinitrogen and argon. J. Hydrol. 208, 16–24.

Blowes, D.W., Ptacek, C.J., Benner, S.G., McRae, C.W.T., Bennet, T.A., Puls, R.W., 2000. Treatment of inorganic contaminants using permeable reactive barriers. J. Contam. Hydrol. 45, 123–137.

Blowes, D.W., Ptacek, C.J., Jambor, J.L., 1997. In-situ remediation of Cr(VI)-contaminated groundwater using permeable reactive walls: Laboratory studies. Environ. Sci. Technol. 31, 3348–3357.

Boudreau, B.P., Westrich, J.T., 1984. The dependence of bacterial sulfate reduction on sulfate concentration in marine sediments. Geochim. Cosmochim. Acta 48, 2502–2516.

Cirpka, O.A., Kitanidis, P.K., 2001. Transport of volatile compounds in porous media in the presence of a trapped gas phase. J. Contam. Hydrol. 49, 263–285.

Daignault, E.C.M., 2002. The Solid Phase Sulphur Speciation of Metal Sulphides in a Permeable Reactive Barrier, Nickel Rim Mine, Sudbury, Ontario. B.Sc. thesis, Univ. Waterloo, Ontario.

Doerr, N., Ptacek, A.C.J., Blowes, D.W., 2005. Effects of a reactive barrier and aquifer geology on metal distribution and mobility in a mine drainage impacted aquifer. J. Contam. Hydrol. 78, 1–25.

Finster, K., King, G.M., Bak, F., 1990. Formation of methylmercaptan and dimethylsulfide from methoxylated aromatic compounds in anoxic marine and fresh water sediments. FEMS Microbiol. Lett. 74, 295–301.

Fortuin, N., Willemsen, A., 2005. Exsolution of nitrogen and argon by methanogenesis in Dutch ground water. J. Hydrol. 301, 1–13.

Fryar, A.E., Schwartz, F.W., 1998. Hydraulic-conductivity reduction, reaction-front propagation, and preferential flow within a model reactive barrier. J. Contam. Hydrol. 32, 333–351.

Guiguer, N., Franz, T., 1997. Visual MODFLOW for Windows v. 2.7.2. Waterloo Hydrogeologic, Inc., Waterloo, Ont., Canada.

Herbert, R.B., Benner, S.G., Blowes, D.W., 2000. Solid phase iron–sulfur geochemistry of a reactive barrier for the treatment of mine drainage. Appl. Geochem. 15, 1331–1343.

Johnson, R.H. 1993. The Physical and Chemical Hydrogeology of the Nickel Rim Mine Tailings, Sudbury, Ontario, M.Sc. thesis, Univ. Waterloo, Ontario.

Kamolpornwijit, W., Liang, L., West, O.R., Moline, G.R., Sullivan, A.B., 2003. Preferential flow path development and its influence on long-term PRB performance: column study. J. Contam. Hydrol. 66, 161–178.

Mackenzie, P.D., Horney, D.P., Sivavec, T.M., 1999. Mineral precipitation and porosity losses in granular iron columns. J. Haz. Mater. 68, 1–17.

Mayer, K.U., Benner, S.G., Blowes, D.W., 2006. Process-based reactive transport modeling of a permeable reactive barrier for the treatment of mine drainage. J. Contam. Hydrol. 85, 195–211.

Mayer, K.U., Blowes, D.W., Frind, E.O., 2001. Reactive transport modeling of an in situ reactive barrier for the treatment of hexavalent chromium and trichloroethylene in groundwater. Water Resour. Res 37, 3091–3103.

Mayer, K. U., Frind, E. O., Blowes, D. W., 2002. Multicomponent reactive transport modeling in variably saturated porous media using a generalized formulation for kinetically controlled reactions. Water Resour. Res. 38, doi: 10:1029/2001WR000862.

Morrison, S.J., 2003. Performance evaluation of a permeable reactive barrier using reaction products as tracers. Environ. Sci. Technol. 37, 2302–2309.

Roychoudhury, A.N., Viollier, E., van Cappellen, P., 1998. A plug flow-through reactor for studying biogeochemical reactions in undisturbed aquatic sediments. Appl. Geochem. 13, 269–280.

Schipper, L.A., Vojvodić-Vuković, M., 2001. Five years of nitrate removal, denitrification and carbon dynamics in a denitrification wall. Water Res. 35, 3473–3477.

Soares, M.I.M., Belkin, S., Abeliovich, A., 1988. Biological groundwater denitrification: laboratory studies. Water Sci. Technol. 20, 189–195.

Soares, M.I.M., Braester, C., Belkin, S., Abeliovich, A., 1991. Denitrification in laboratory sand columns: carbon regime, gas accumulation and hydraulic properties. Water Res. 25, 325–332.

Stumm, W., Morgan, J.J., 1996. Aquatic chemistry, third ed.Chemical Equilibria and Rates in Natural Waters Wiley, New York, pp. 472–474.

Vikesland, P.J., Klausen, J., Zimmermann, H., Roberts, A.L., Ball, W.P., 2003. Longevity of granular iron in groundwater treatment processes: changes in solute transport properties over time. J. Contam. Hydrol. 64, 3–33.

Waybrant, K.R., Blowes, D.W., Ptacek, C.J., 1998. Selection of reactive mixtures for use in permeable reactive walls for treatment of mine drainage. Environ. Sci. Technol. 32, 1972–1979.

Waybrant, K.R., Ptacek, C.J., Blowes, D.W., 2002. Treatment of mine drainage using permeable reactive barriers: column experiments. Environ. Sci. Technol. 36, 1349–1356.

Westrich, J.T., Berner, R.A., 1984. The role of sedimentary organic matter in bacterial sulfate reduction: the G model tested. Limnol. Oceanogr. 29, 236–249.

Williams, R.L., 2005. Using Dissolved Gas Analysis to Investigate the Performance of Permeable Reactive Barriers, M.A.Sc.-thesis, Univ. British Columbia, Vancouver.

Yamamoto, S., Alcauskas, J.B., Crozier, T.E., 1976. Solubility of methane in distilled and sea water. J. Chem. Eng. Data 21, 78–80.